frontiers | Frontiers in Earth Science

TYPE Original Research
PUBLISHED 19 August 2024
DOI 10.3389/feart.2024.1377997

OPEN ACCESS

EDITED BY
Ángel Puga-Bernabéu,
University of Granada, Spain

REVIEWED BY
Pere Puig,
Spanish National Research Council (CSIC), Spain
Cheng-Shing Chiang,
National Museum of Natural Science, Taiwan
Guangfa Zhong,
Tongji University, China

*CORRESPONDENCE
M. Elliot Smith,
michael.e.smith@nau.edu

RECEIVED 28 January 2024
ACCEPTED 22 July 2024
PUBLISHED 19 August 2024

CITATION
Joerger ST, Smith ME, Buscombe D and Mueller ER (2024), Evidence for littoral convergence and sediment delivery to Mattole submarine canyon, Northern California.
Front. Earth Sci. 12:1377997.
doi: 10.3389/feart.2024.1377997

Evidence for littoral convergence and sediment delivery to Mattole submarine canyon, Northern California

Sarah T. Joerger[1], M. Elliot Smith[1]*, Daniel Buscombe[1,2] and Erich R. Mueller[3]

[1]School of Earth and Sustainability, Northern Arizona University, Flagstaff, AZ, United States, [2]Marda Science LLC, Santa Cruz, CA, United States, [3]Department of Geosciences, Southern Utah University, Cedar City, UT, United States

At geologic timescales, a significant proportion of the sediment eroded from continents is transferred from rivers to littoral cells, then through submarine canyons to deep ocean basins. Accumulation and occasional discharge of sediment from canyon headwall regions is a likely driver for the sediment gravity flows believed to be responsible for much of this mass transport, but the responsible mechanisms and event timescales in canyon heads are imprecisely defined, largely due to the drowning of canyon heads since the last glaciation and the resulting dearth of modern depositional environments to observe. We investigated a littoral cell adjacent to Mattole submarine canyon in Northern California to better understand the influence of bathymetry and coast shape on sediment trajectories and hypothesize that canyon heads promote littoral sediment accumulation due to bathymetric sheltering of the adjacent coast from waves and convergence of littoral cells exposed to varying wave direction. The uppermost gullies of Mattole Canyon extend to the littoral cell, and a train of sediment waves within the uppermost thalweg of Mattole Canyon suggests that gravity-driven flows of shore-derived sediment may have recently occurred. Mattole Canyon and nearby Mendocino Canyon flow into the deep Mendocino Channel, which has the highest observed Late Holocene sediment accumulation rates in Northern California. We documented the beach slope, grain size, and sediment provenance along 15 km of coast adjacent to Mattole Canyon and conducted numerical wave modeling to infer the dominant direction and magnitude of sediment transport, relative wave sheltering by bathymetry, and estimated sediment mobility in the vicinity of the canyon head over a multi-year period. South of the canyon headwall, in the vicinity of the Mattole River outlet, coarser sediment rich in metasandstone clasts and steeper beach slopes coincide with decadal-scale beach accretion. North of the canyon head, sediments are generally finer, beaches are flatter, clast lithologies include more quartz and mudstone grains, and there is decadal-scale net erosion. Wave modeling suggests the Mattole headwall region is subject to sustained sheltering from waves due to canyon bathymetry, littoral sediment convergence above the canyon head for much of a typical year, and occasional bed entrainment of sediment in the canyon's uppermost gullies by large waves. Larger winter waves from the northwest likely result in net southerly drift north of the canyon head, with a high likelihood of preferentially transporting fine-grained, more quartz-rich sediment towards the Mattole headwall. Smaller summer swells from the

west and south likely results in net northerly transport of metasandstone clast-rich Mattole River-derived sediment towards the canyon head. The imbalance in seasonality in wave conditions, coast shape, and sediment delivery by the Mattole River and other coastal creeks is broadly consistent with the spatial patterns in grain size, mineralogy, slope, and beach width that we observe in the vicinity of the canyon, and the net delivery of sediment to the Mattole Canyon head. An approximate mass balance of sediment flux from coastal streams feeding Mattole River littoral cell suggests that sediment volumes likely accumulate in the canyon headwall region that could supply several density flow events in a typical decade. These findings highlight the importance of the connectivity of the canyon to the nearshore region for the processes and products in canyons and fans. We hypothesize that feedbacks between canyon bathymetry, sediment accumulation, and mass evacuating flows promotes the long-term persistence of canyon systems.

KEYWORDS

submarine canyon heads, beaches, littoral cells, wave refraction, provenance, sediment transport

1 Introduction

Submarine canyons are common features of continental shelves and serve as conduits for terrigenous sediment to deep ocean basins (Paull et al., 2011; Covault et al., 2014). The regular occurrence of turbidity currents and subaqueous debris flows is likely to be the primary control on canyon formation and grading (Shepard, 1981; Talling et al., 2015; Symons et al., 2016), but are difficult to study due to the rarity of shore-connected canyons following drowning by Holocene sea level rise, and the difficulty in instrumenting in these high-energy environments. Turbidity currents and subaqueous debris flows can transport sediment down the axis of a canyon, and are often deposited as fan complexes down-gradient (Lamb et al., 2008; Romans et al., 2011; Covault and Fildani, 2014). Shore-connected canyons on open coasts around the world are often connected to fluvial sources by transport within littoral cells (Lewis and Barnes, 1999; Arzola et al., 2008), but the various roles of nearshore canyons on nearshore coastal processes such as wave transformation and gradients in sediment transport are not well understood (Bernhardt and Schwanghart, 2021). For example, while canyons are known to modify the spatial distribution of wave energy over a range of conditions (Ortega-Sánchez et al., 2014; Hansen et al., 2015), it is not generally known under what circumstances canyon headwalls intercept and capture sediment in transport in the littoral zone. Sediment enters the littoral cell from coastal streams and from erosion of coastal cliffs, bluffs, and beaches. Some proportion of this material is, at least over geologic timescales, intercepted and exported from the shelf by submarine canyons whose headwalls are in sufficiently shallow water (Patsch and Griggs, 2007; Covault et al., 2011; Ortega-Sánchez et al., 2014). A correlation between coarse fluvial sediment delivery to the littoral zone, onshore relief, and submarine canyon occurrence suggests that sediment transport may promote submarine incision and channel maintenance (Pratson and Coakley, 1996; Smith et al., 2017; Bernhardt and Schwanghart, 2021), and the generation and propagation of knickpoints (Chen et al., 2021; Guiastrennec-Faugas et al., 2021). Presumably, greater fluxes of sediment should trigger larger, more frequent mass transport events (Clare et al., 2016). Repeat multibeam surveys in high sediment transport locations at the delta fronts of the Squamish and Fraser rivers in British Columbia, where turbidity currents are routinely generated by surface plumes and by mass failures, which results in daily to weekly migration of crescentic bedforms (Lintern et al., 2016; Hage et al., 2019). Less is known about turbidity current generation and processes in canyons connected to littoral systems, but bed agitation and fluidization of muddy sediment by waves and seismicity are among several important triggering mechanisms for generating density currents (Paull et al., 2003; Goldfinger et al., 2007; Palanques et al., 2008; Talling, 2014; Normandeau et al., 2019). At tectonically active coasts, ground shaking during major earthquakes has been shown to trigger the largest, most far-traveled turbidity currents (Goldfinger et al., 2007; Mountjoy et al., 2018). In most of the cases outlined above, sediment supply and the grade and stability of resulting slopes is a key consideration for whether a particular river plume, wave field, or earthquake succeeds in triggering a current.

Numerical wave modeling of wave transformation over submarine canyons shows that submarine canyon bathymetry can enhance wave-generated bottom currents within the canyon heads, and also shelter the adjacent shore from wave energy, promoting sediment accumulation (Long and Özkan-Haller, 2005; Magne et al., 2007; Thomson et al., 2005; Gorrell et al., 2011; Hansen et al., 2015; Hansen et al., 2017; Smith et al., 2018). These effects are often highly localized because canyon headwall regions tend to be narrow (tens to hundreds of meters in alongshore extent); with sheltering effects depending on numerous factors such as canyon bathymetry and shoreline orientation with respect to the dominant wave direction(s), and the availability of littoral-grade sediment. However, with few high-resolution observations of shore-connected canyon headwalls and even fewer time-series of mass transport events, the specific relations between forms and the processes that shape them are largely unknown.

In this contribution, we present the results of investigation of the character of a shoreline adjacent to a submarine canyon with a

shallow headwall: the Mattole submarine canyon offshore of Northern California, and consider the evidence of co-evolution of canyon and the adjacent regional coastline morphology. For the purposes of this study, shallow water is considered to be less than half the wavelength of offshore waves, therefore, at this location around 30 m water depth, since a typical wave period for this location of ~7 s results in a ~60 m-long wave. To carry out this investigation, we characterized the littoral cell adjacent to the canyon using sedimentary provenance, cross- and alongshore transects of grain-size and beach slope, satellite imagery, published shoreline change rates for this location, and numerical wave modeling to better understand the processes at work in a shore-connected submarine canyon system.

1.1 Mattole Canyon

Mattole Canyon head occupies a west-facing portion of coast south of Cape Mendocino in Northern California that is coincident with the Mendocino Triple Junction (Figure 1). The region is predominantly impacted by waves from the west and northwest during a typical year (Figure 2A). Mattole Canyon and nearby Mendocino Canyon are tributaries to the deep Mendocino Channel, which extends into the 2,750 m deep Gorda Basin adjacent to the Mendocino Fracture Zone escarpment (Goldfinger et al., 2012; Gardner, 2017) (Figure 1). A core of ^{14}C-dated sandy turbidites deposited in the Mendocino Channel at 2621 m depth (site M9907-51PC of Goldfinger et al., 2012) during the last millenium has the highest recorded sediment accumulation rate (Figure 1B) and the shortest turbidite recurrence interval (23 years on average) of all cored deep-water channels offshore Northern California and Oregon (Goldfinger et al., 2007; Goldfinger et al., 2012). The thalweg of Mattole Canyon follows a major transform a fault below 800 m depth (Figure 1A), but does not follow any major fault in its meandering upper canyon (Figure 2A). Several gullies that extend to 10–15 m water depth within 250 lateral meters of the beach coalesce down-gradient into a single thalweg at approximately 60 m depth, (Figure 2B). At the water depth of these uppermost headwall gullies, large ocean waves are known to entrain significant amounts of sediment, which is evidenced by wave-scoured bedrock on the shelf adjacent to Mattole Canyon (Figure 2C). The depth limit of wave-driven sediment resuspension, known as the "depth of closure" (Hallermeier, 1981) was estimated to be 17–18 m in the Klamath River littoral cell, located approximately 140 km to the north of the present study area but with similar wave exposure (Warrick et al., 2023). Two hanging tributary gullies are oriented toward the Mattole River outlet and join the thalweg from the southeast 2 and 3 km from shore, and begin at 40 and 60 m depth, respectively (Figure 2C). While these gullies are likely below the typical depth of closure for bedload, they may be shallow enough to collect wave-driven fluid mud from the shelf, as has been observed adjacent to the Eel Canyon head at 60 m water (Puig et al., 2003).Waves likely triggered a ROV-observed dilute turbidity in nearby Mendocino Canyon (Sumner and Paull, 2014), which extends to 100 m depth (Figure 1A). A 2008 multibeam sonar survey of Mattole Canyon by the California Seafloor Mapping Project (Johnson et al., 2017) revealed the presence of 40–80 m-spaced sediment waves within the canyon thalweg (Figure 2C), which may suggest recent down-canyon sediment transport from the littoral cell (Sequeiros et al., 2010; Covault et al., 2017).

High relief and high sediment supply to the shore near Mattole Canyon results from uplift generated where the North American and Pacific plates are locally in convergence on the east side of the Mendocino Triple Junction (Figure 1; McLaughlin et al., 1982; Furlong and Schwartz, 2004; Lock et al., 2006). The region experiences regular seismicity (Figure 1A) and among the fastest uplift rates of any site in the contiguous U.S. (McLaughlin et al., 1983; Merritts and Bull, 1989; Dumitru, 1991; Moon et al., 2018). Bedrock underlying the study area consists of the youngest unit (or terrane) of the Coastal Belt Franciscan metamorphic complex (Dickinson and Snyder, 1979; McLaughlin et al., 2000) and overlying Cenozoic marine sedimentary strata (Dibblee, 2008).

There is no direct fluvial input to Mattole Canyon, evidenced by the 1 km lateral displacement between the canyon headwall and the Mattole River outlet (Figure 1A). Rather, sediment delivered by coastal streams is transported alongshore, then cross-shore to enter its uppermost gullies. Stream outlets and bluff erosion feed the Mattole River littoral cell (Patsch and Griggs, 2007), which is separated from the adjacent Eureka and Spanish Flats littoral cells by headlands to the north and south, respectively (Figure 2A). The perennial Mattole River has the largest (789 km^2) catchment of all rivers feeding the Mattole River littoral cell (Figure 2A) and delivers to the shore an average estimated bedload of 30,000 tons/year and suspended load (i.e., particles <1 mm) of two million tons/year (Andrews and Antweiler, 2012). Most sediment transport to the ocean from the Mattole River occurs during and following winter and spring storms. This is evident in the Mattole River stream gage (USGS gage 11468990) record, which showed 2 to 10 flood pulses of 300–1,000 m^3/s each winter during the 4 years prior to the field study for this work in summer 2019. Mattole River flows often fall to less than 1 m^3/s in summer and early fall, allowing beach sediment to close the estuary. The outlet of the Mattole River undergoes transitions from closed to open depending on the discharge/precipitation within the watershed, leading to intermittent sediment supply to the nearshore coastal ocean (Figure 3). Other smaller coastal streams that empty into the littoral cell are estimated to collectively deliver approximately 6,000 tons/year of bed load sediment to the shore (Smith et al., 2017). A relatively smaller amount of sediment may enter the cell, based on a recent short-term coastal cliff and bluff erosion study (Swirad and Young, 2022).

The mean spring tidal range at the study location is 2.9 m, and the mean annual significant wave height is 2.3 m (Hersbach et al., 2020), which in a global context is moderately high wave energy (Sayre et al., 2019). The beaches are composed of coarse mixed clastic material, and the location is classified as neither cross-shore nor alongshore dominant by Vitousek et al. (2023), which means the beaches neither display classic seasonal behavior in summer-winter profiles (Bascom, 1951), nor do alongshore gradients in sediment transport dominate the short-term seasonality signal like they do on many alongshore-uniform sand beaches. In a recent California-wide assessment of long-term (1995–2020) shoreline trends based on satellite-derived shoreline detection (Vos et al., 2023) and data assimilative shoreline modeling (Vitousek, 2023), beaches of the Mattole River littoral cell were found to have modest positive

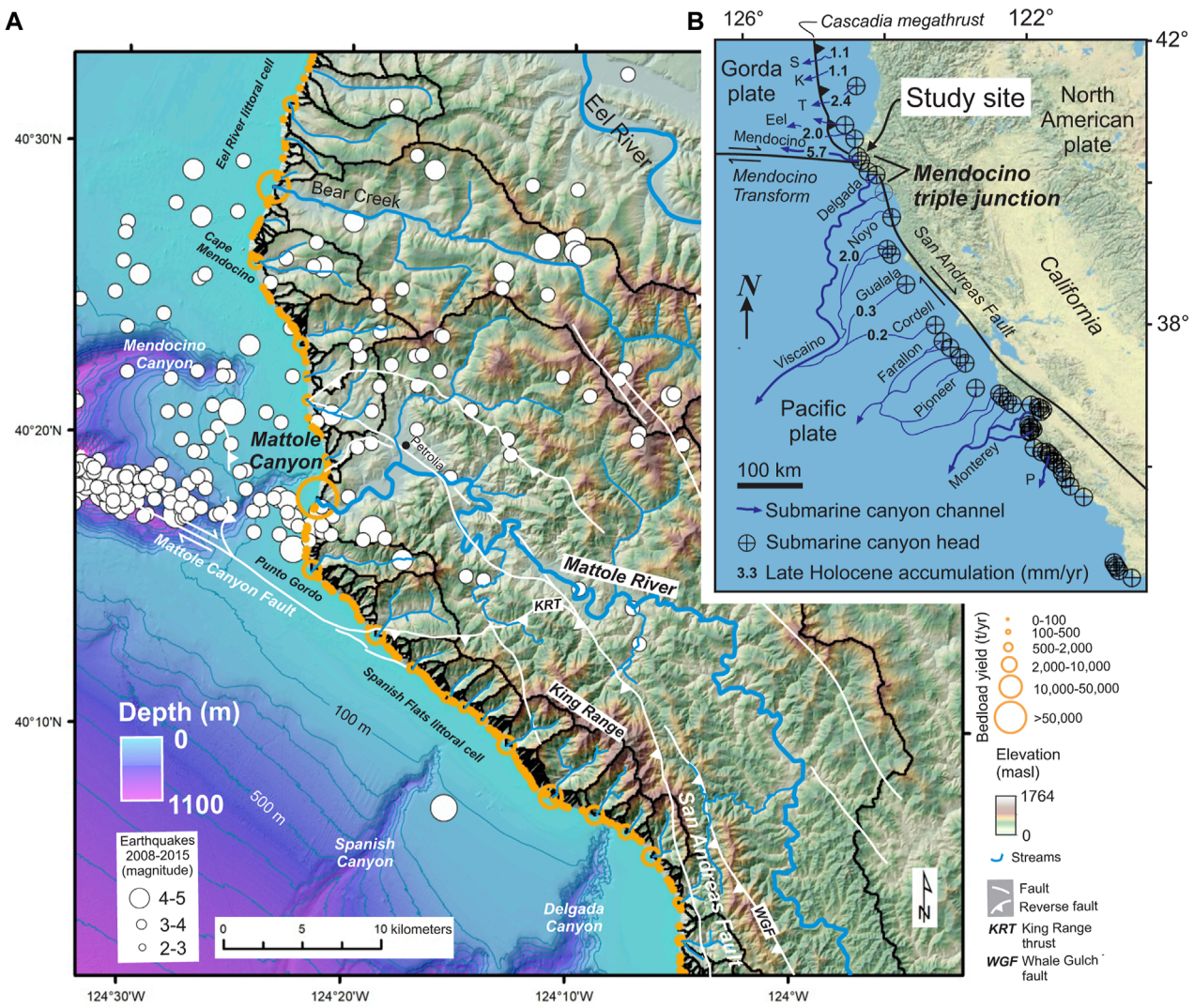

FIGURE 1
Tectonic and physiographic setting of Mattole Canyon: **(A)** Map showing topography, faults, submarine canyons, earthquake epicenters (2008–2015), and modeled sediment yields at the Mendocino Triple Junction coast, modified from Smith et al. (2018); **(B)** Regional tectonics and submarine canyons and channels offshore Northern and central California, showing ^{14}C-based sediment core-measured sediment accumulation rates for the last 800–1,200 years from Goldfinger et al. (2007) and Goldfinger et al. (2012). Labeled submarine canyons: S-Smith; K-Klamath; T-Trinidad; P-Partington. Shore-connected canyons and channels are shown with thicker line widths.

shoreline change rates of 0.3–0.4 m/year (Vos et al., 2023), whereas some rocky shorelines in the littoral cell experienced net coastal erosion of up to 2 m (Vitousek et al., 2023). Based on analysis of published satellite-derived shoreline position time-series data at this location (Vos, 2023), there are no detectable coherent sediment waves (so-called shore-connected "accretion waves") propagating along this coast, unlike elsewhere in the region (Warrick et al., 2023). The obvious source of externally-sourced sediment waves would be the Eel River in the Eureka littoral cell to the north, but it is believed that most of this predominantly fine sediment is lost offshore on the continental shelf or to the Eel submarine canyon (Mullenbach et al., 2004; Patsch and Griggs, 2007), so alongshore contributions of sediment to the Mattole cell from adjacent littoral cells are hereafter considered negligible. Subsea seismic imagery of Late Neogene strata on the shelf adjacent to Mattole Canyon shows minimal sediment accumulation (Beeson et al., 2017), consistent with the capture and removal of sediment from the shoreface by Mattole Canyon.

2 Methods

2.1 Beach morphology and grain size

To document beach characteristics, we measured beach slope, surface and subsurface grain size, and subsurface sediment composition across 15 km of coast, from approximately 4 km south of the Mattole River outlet to approximately 11 km north of the outlet (Figure 4). We also examined the Sentinel-2 (S2) satellite image record for the period 2017-08-26 (the earliest

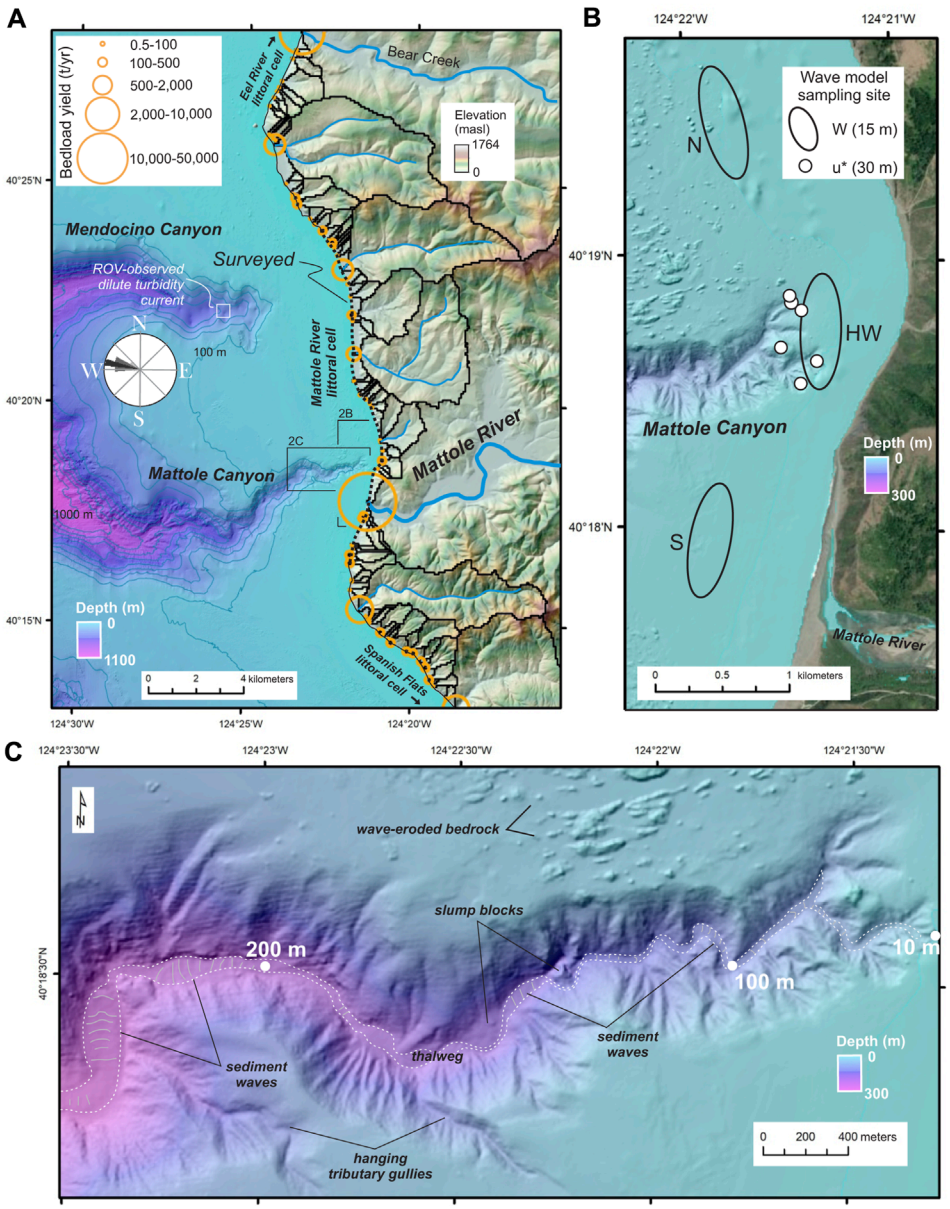

FIGURE 2
(A) Map of the Mattole River littoral cell and adjacent bathymetry and topography; ROV observation site in Mendocino Canyon (Sumner and Paull, 2014) is labeled; **(B)** the Mattole Canyon head; white dots and ovals show locations where modeled wave-driven currents shown in Figure 6 were averaged from; HW indicates headwall; **(C)** the uppermost 250 m of Mattole Canyon, showing meandering thalweg with sediment waves, in-canyon slump features, and the wave-scoured adjacent shelf.

cloud-free S2 image) to 2019-08-31, over a similar spatial extent (examples shown in Figure 3). This provided information such as the variability in shoreline position, beach width, and the path of suspended sediment plumes, and qualitative information such as the likelihood of waves impacting cliffs over a multi-year period. Field surveys were conducted in summer 2019. Sediment samples were collected and cross-shore beach elevation transects were measured at 30 sites spaced 500 m apart using a survey rod and hand level (Figure 4). Beachface slopes were measured from water's edge to approximately 2 m past the high-water line every 5 m along each transect, and also at breaks in slope on the supratidal portion of the beach. Photographs of the surface beach sediment were taken to characterize the current sediment being actively mobilized. A sediment sample was collected from the midpoint of each survey site, corresponding to approximately mean high water, following the procedures outlined in Mueller et al. (2016). Grain sizes of >22.6 mm in diameter were characterized for grain size and lithology in the field with a gravelometer and hand lens. The remaining sediment (≤22.6 mm in diameter) was subsampled and taken to the lab for further grain-size and compositional analysis (Supplementary Table S1). Photos for grain-size analysis were taken on cross-shore transects at regular 5 m spacing orthogonal to the beach surface following the field methods of Warrick et al. (2009) and the photogrammetric grain

10.3389/feart.2024.1377997

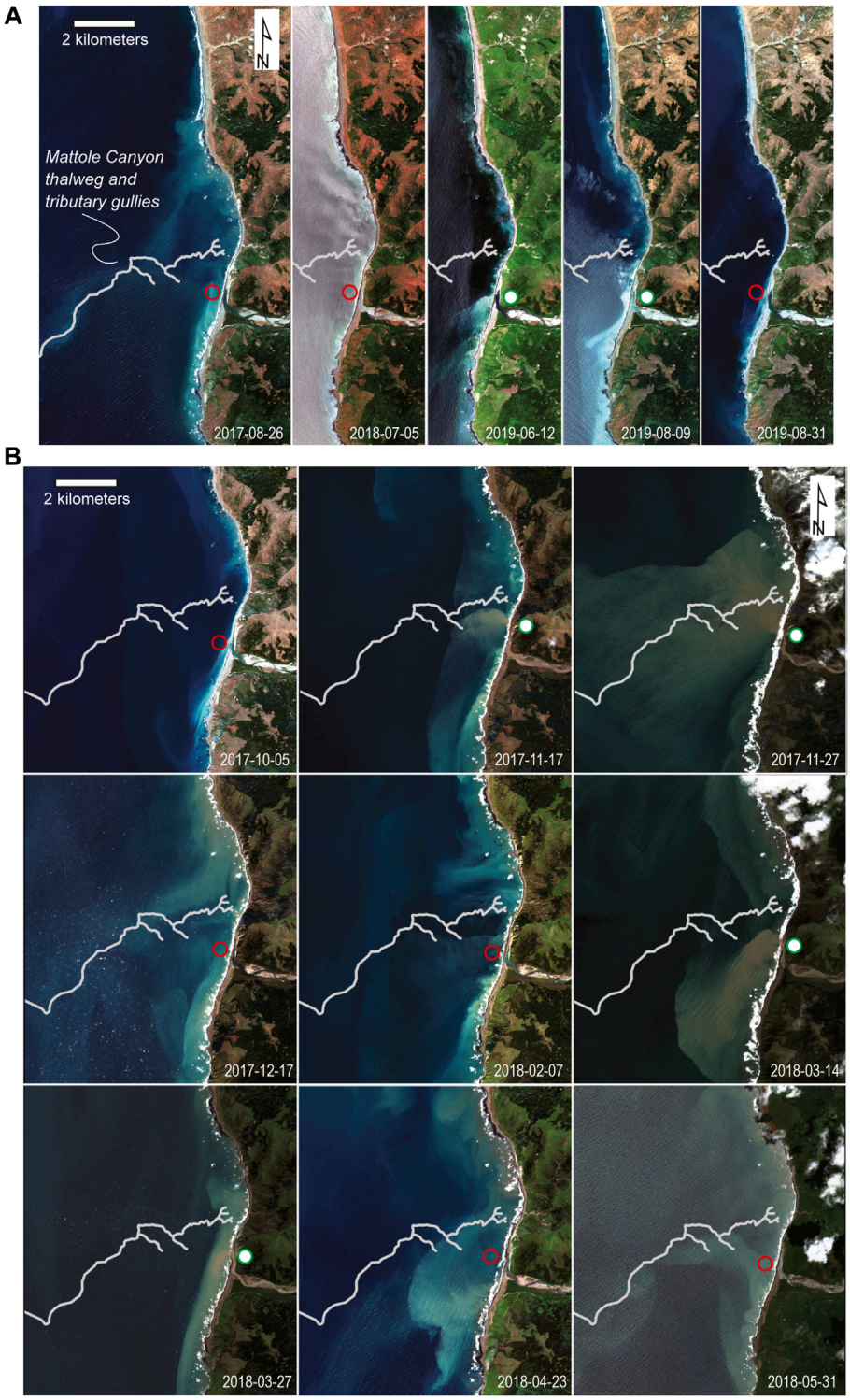

FIGURE 3
Satellite data constraining shoreline changes, beach morphology, and wave and river-generated sediment plumes,: **(A)** Sentinel-2 satellite image time series of the Mattole River littoral cell under relatively low wave conditions and near low tide from 2017 to 2019. A red circle indicates a closed river outlet, whereas a green circle indicates an open river, with the circle position indicating the outlet position; **(B)** A time-series of Sentinel-2 imagery taken during the 2017–2018 rainy season showing varying river outputs, wave conditions, and the position of suspended sediment plumes.

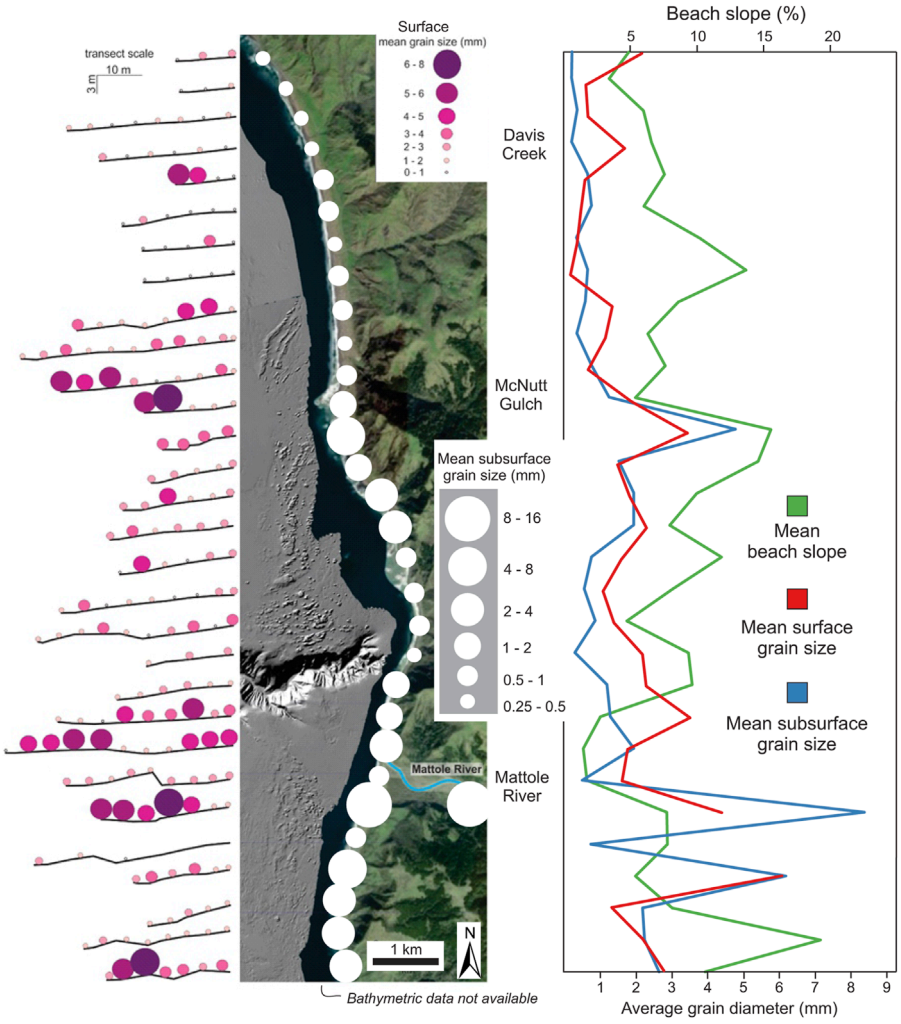

FIGURE 4
Results of beach surveys, showing mean slope and mean grain size for surface and subsurface sediment.

size estimation method of Buscombe (2020) (Figure 4). The grain-size estimation technique uses a convolutional neural network to estimate certain percentiles of the cumulative grain size distribution from the photographic images. It is evaluated and fine-tuned using some manual on-screen clast diameters of representative images (Warrick et al., 2009; Buscombe, 2020), with estimated median grain sizes within 15% error. To characterize sediment sources, bulk sediment samples were collected from the Mattole River, smaller coastal drainages, and coastal bluffs with evidence of mass wasting.

2.2 Geochemistry and provenance

To qualitatively infer the provenance of beach sediment, sediment samples collected across the study area of the 4–2 mm, 2–1 mm, and 1–0 mm size fractions were analyzed for elemental composition using a handheld Niton XL3 GOLDD X-ray fluorescence analyzer (pXRF) in "mining mode." The device bombards a sample with X-rays and simultaneously measures secondary X-rays that are characteristic of particular elements. Variations in bedrock lithology within catchments can lead to measurable differences in sediment elemental concentrations that have proven useful for tracking sedimentary provenance (Smith et al., 2018; Chapman et al., 2021; Kemper et al., 2022). Sieved sediment size fractions from each sample were analyzed separately to compare elemental compositions of different grain sizes. Each sample was analyzed three times for 150 s per run and rotated between each analysis to obtain an accurate average value. Elemental concentrations of Mg, Al, Si, P, S, Ba, Cl, K, Ca, Ti, V, Cr, Mn, Fe, Co, Ni, Cu, Zn, As, Rb, Sr, Zr, and Nb were collected for three grain size fractions of each sample (Supplementary Table S2). Principal components analysis (PCA) was used to analyze variance in pXRF acquired element concentrations to map compositional differences across the beach (Figure 5A). Sediments with grain sizes of 1 phi or larger were point counted using a binocular microscope to identify differences in lithology and compare with pXRF results. Thin sections of select samples of 0.5–1 mm sand were also point counted using a petrographic microscope to identify differences in mineralogy and calibrate pXRF results (Figure 5B; Supplementary Table S3).

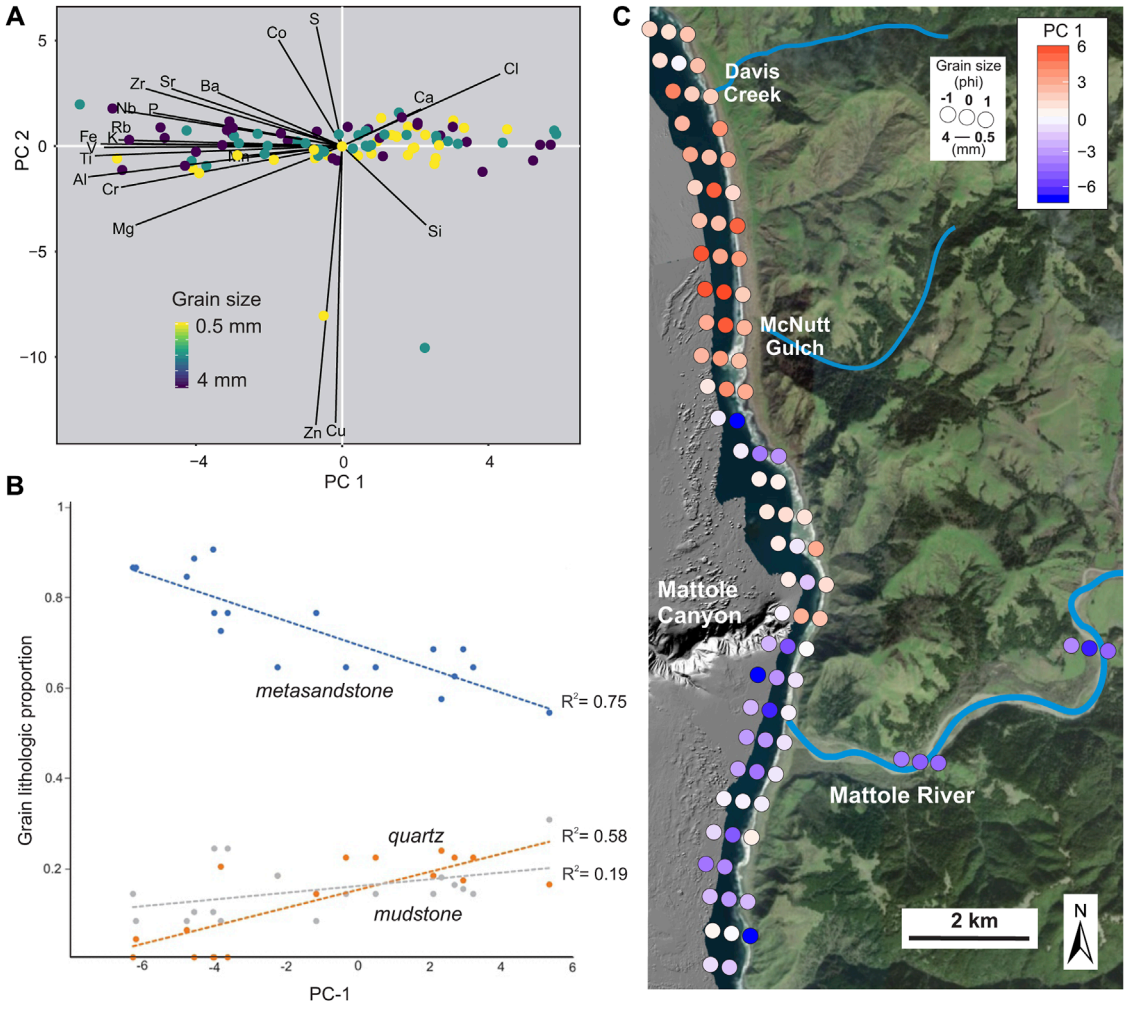

FIGURE 5
Sediment provenance: **(A)**: PCA results; **(B)** regressions of point counts with PC1 values. **(C)** Map showing grain size and XRF-based compositional variation across the Mattole River-Mattole Canyon system, showing average grain size and the first principal component (PC-1) of 16 XRF-measured element concentrations in 1–2 mm sediment. Note that Mattole River sediment (cool colors) progressively fines and mixes with sediment derived from coastal creeks to the north (warm colors) near Mattole Canyon.

2.3 Numerical wave modeling

We used numerical wave modeling of the interaction between the submarine canyon bathymetry and waves to understand differences in wave energy, wave direction, and wave-driven sediment transport in the vicinity of the Mattole headwall during the year prior to littoral sediment sampling (2017–2018). We used the Simulating Waves Nearshore (SWAN) model, a two-dimensional hydrodynamic model that models wave transformation over complex bathymetry (Booij et al., 1999; Zijlema and van der Westhuysen, 2005; Zijlema, 2010). Inputs for SWAN include local tide tables and the outputs of NOAA's regional wave model Wavewatch III (Tolman, 2009), itself forced by NOAA buoy stations 46,014, 46,213, and 46,022. The grids for SWAN were created using bathymetry from the California Seafloor Mapping Program (2008). Grid cells are 13 m by 13 m, chosen considering the bathymetric data resolution and model convergence stability. The model was forced at the computational boundary using wave time-series from Wavewatch III, but was not validated or calibrated with inshore measurements, which are not available at or near this location. In lieu of an optimal method for model calibration (Amarouche et al., 2021; Wu et al., 2021) and *in situ* measurements of waves and currents, we use uncalibrated model outputs. Several studies (e.g., Beyramzadeh et al., 2021) have reported a general lack of sensitivity of tuning on bulk wave parameters (e.g., significant wave height and direction) especially in high energy conditions on open coasts, such as here. We therefore used the model outputs in the same way as Smith et al. (2018), to provide a synoptic qualitative insight into the alongshore and temporal distribution of wave energy that emerges due to complex offshore bathymetry and offshore wave forcing.

Alongshore power (W) can be used to model longshore transport capacity for sand and gravel and was calculated using the methods of van Rijn (2014), where $W = \sin(2\theta) * H^3$, where θ is the wave incidence angle and H is wave height (Figure 6A). Model outputs are used to show spatial differences in wave power either side of the canyon headwall. Power was calculated for the

headwall (W_{HW}), north (W_N), and south (W_S) from the canyon (Figure 2B). For each, values of W were averaged from five locations along the 15 m isobath to remove potential bias in point selection. Where values are positive, transport is to the south direction, whereas negative values indicate transport to the north. To visualize wave model outputs, we consider four theoretical scenarios for directions of sediment transport in and around the canyon head in a quadrant plot (Figure 6B). In scenario one, the upper right quadrant, locations to the north (W_N) and south (W_S) have positive values implying there is net longshore sediment transport to the south. In scenario two, the lower left quadrant, values at both locations are negative causing net longshore transport to the north. In scenario three, the lower right quadrant, W_N is positive and W_S is negative, which should lead to convergence of littoral sediment. The fourth scenario, not observed in the data considered, would occur when W_N is negative and W_S is positive where sediment would diverge from the canyon head.

Sheltering of the canyon head can occur when wave forces are weaker in the canyon head than on the adjacent shelf, potentially leading to the accumulation of sediment. An index of sheltering (Sh) was calculated using the equation $Sh = \log(W_N+W_S/2W_{HW})$ where larger values indicate a higher degree of sheltering of the headwall and negative values indicate focusing of waves in the canyon head (Figure 6D). We also calculated bed shear velocity (u^*) at five locations at 30 m depth within the canyon head using the methods described in Smith et al. (2018) to assess the role of waves in sediment mobilization that may affect the generation of gravity-driven flows (Figure 6C).

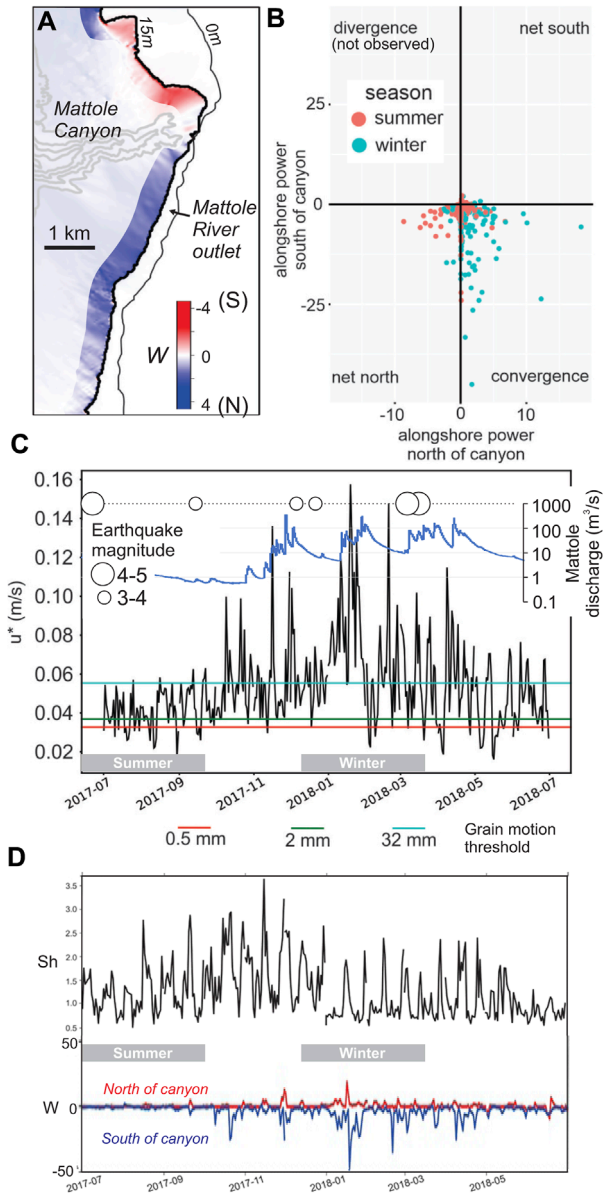

FIGURE 6
Outputs from a SWAN (Booij et al., 1999) nearshore spectral wave-transformation model, forced by regional WaveWatch III (Tolman, 2009) model outputs-: **(A)** Alongshore wave power ($W = H_{rms}^3 \sin\theta_{br}$, where H_{rms} and θ_{br} are, respectively, root mean squared wave height and direction relative to shore, at wave breaking) computed in the nearshore region of the SWAN model domain up to the 10 m isobath, December 17–24, 2019; **(B)** Distribution of alongshore current north and south of the canyon head (July 2017–July 2018); **(C)** Distribution of modeled shear velocity, u^*, within the Mattole Canyon head (July 2017–July 2018), compared with Mattole River discharge and local seismicity (BDSN, 2014). Horizontal lines reflect critical Shields stress threshold for different sediment size classes, computed according to the Buscombe and Conley (2012) criterion that accounts for relative sheltering effects in mixed sand-gravel sediment; **(D)** Sheltering (Sh) and sediment transport direction (W) values across the same time period.

3 Results

3.1 Beach morphology

Beachface slopes within the Mattole River littoral cell range from 2% to 20%, with an average slope of 8% (Figure 4). Beach profiles vary from flat beaches for the northernmost transects, steep beaches with prominent slope breaks or berms north and south of the canyon head, and a flat, narrower beach immediately adjacent to the head of the Mattole Canyon. Beach sediment ranges from cobble to medium sand size and is poorly to moderately sorted. Beach sediment is coarsest adjacent to river and creek outlets. Surface and subsurface grain sizes are generally similar to one another, i.e., beach surfaces are not generally armored; a regression of average surface and subsurface grain sizes across the sampling locations has an R^2 value of 0.64. A lack of armoring is a strong indication of mixing due to regular sediment transport of the majority of clast sizes in this energetic wave environment. Beach sediment in the vicinity of the Mattole River outlet is generally coarse and composed of predominantly granule and pebble sized clasts, while sediment to the north is finer grained and consists predominantly of medium to coarse sand, except immediately adjacent to the outlets of coastal creeks (Figure 4). Sediment immediately adjacent to the head of Mattole Canyon is finer grained than the beach sediments to the north and south. From the 10-m pixel Sentinel-2 satellite image time-series, the widest beaches which, given the observed variability in beach slopes, we assume to be well-correlated with total subaerial sediment volume, are always located south of the Mattole River outlet to the north of the outlet of McNutt Gulch (Figure 5C), whereas the beach is consistently narrower in the embayment adjacent to Mattole Canyon (Figure 3A). The Mattole River outlet is generally open during the rainy season when discharge is high

(Figure 6C), but is often closed for long periods, especially in summer (Figure 3A). Across the rainy season prior to the field survey (Figure 3B), peaks in Mattole River discharge correspond to plumes emanating from its outlet. In most instances, the Mattole River outlet plume is diverted south, but on rare occasions the plume directed northwest towards the canyon head (see image from 2017-11-27). Plumes are also observed originating from the littoral cell, particularly to the north of the canyon head. In several of the images, suspended sediment plumes appear to follow the canyon thalweg out to sea (see images from 2017-08-26, 2017-12-17, and 2018-05-31), suggesting the occurrence of a bathymetry-generated rip current (cf. Long and Özkan-Haller, 2016).

3.2 Provenance

Three main clast lithologies are present in beach sediment in the study area: 1) metasandstone that varies between lithic and arkosic in composition; 2) mudstone or slate that varies from black to green in color; and 3) monomineralic grains of predominantly quartz and feldspar. These lithologies were eroded from the coastal belt Franciscan complex rocks and overlying Cenozoic sedimentary strata that underlie watersheds and bluffs of the region. The average proportion of each lithology across the beach is 71% ± 20% metasandstone, 15% ± 10% mudstone, and 12% ± 10% monomineralic grains (Figure 5B). A PCA of XRF results for sand-sized grains assigns 56% of variance to principal component 1 (PC1) and 32% of the variance to PC2 (Figure 5A). Si, Ca, and Cr concentrations load on PC1 positively, while Mg, Mn, Al, Ti, V, Fe, K, Rb, Nb, Zr, Sr, Ba, and Bi concentrations load negatively. PC2 is correlated positively to Co and S abundance, and negatively to Zn and Cu abundance. Regressions between PC1 and the proportion of different clast lithologies indicate that PC1 is lowest in samples rich in metasandstone clasts derived from the Mattole River, and highest in samples with more monomineralic grains delivered to the system by coastal streams to the north of the canyon head (Figure 5B). This suggests that PC values can be interpreted qualitatively as a provenance indicator. For each grain size fraction analyzed, sediment from north of the canyon head possessed positive PC1 values, whereas sediment from south of the canyon head and Mattole River channel has negative PC1 values, and sediment adjacent to the canyon head was mixed in PC1 value (Figure 5C).

3.3 Wave modeling

Modeled wave and sediment transport indicate that values for W north, south, and at the head of the canyon vary from positive to negative at each location, indicating varying net north, net south, and longshore convergence across a typical year, depending on wave direction. For the year investigated, longshore convergence was the most common transport scenario (Figure 6B). Convergence occurs primarily when there is a western-northwestern swell, between 270 and 300 degrees, but it can also occur when waves come from a more northerly or southerly direction. The highest Sh values occurred primarily in the fall, with lower values throughout the rest of the year (Figure 6D). Focusing of wave energy in the canyon head is most common during the winter months, and results in wave generated currents capable of mobilizing fine gravel down to perhaps 30 m depth or more (Figure 6C). Even if our wave-generated current velocities are over-estimates, fine gravel mobilization down to at least the uppermost gullies of Mattole Canyon is plausible, if not likely.

4 Discussion

The differences we observed in slope across the beach likely result from the combined influence of varying supply of coarse sediment and the seasonal interplay of dominant wave forcing. Grain size maxima occur adjacent to the outlets of coastal streams, particularly the Mattole River, which likely reflects proximity to relatively coarse fluvial source material. It is less likely that significant amounts of large grain sizes also result from debris shed from bluffs and cliffs behind the beach to the south of the river outlet, because cliff erosion rates here are very low (Swirad and Young, 2022), beaches are consistently wider to the south of the river than to the north (Figure 3A), and the long-term shoreline trend at this location is moderate accretion (Vitousek et al., 2023). The differential in shoreline trend on either side of the river outlet, as well as the wider beaches south of the outlet, both suggest long-term net southerly transport owing to a dominance of winter waves. However, satellite imagery reveals that northerly beaches also appear to recover in the summer, and the river outlet often tends to hook north in spring and summer months, perhaps suggesting of northward sediment transport for certain times of year under westerly or south-westerly waves. A general correlation between grain size and beach slope such as was observed across the study area (except at the Mattole River outlet location, as described above; Figure 4) has been interpreted by previous workers to reflect a higher angle of repose for coarse sediment allowing for steeper slopes (Bascom, 1951; Wright et al., 1985). A regional minimum in slope and grain size occurs behind the head of the canyon, consistent with locally diminished wave conditions that we interpret to result from sheltering.

Petrography and geochemical provenance data for beach sediment suggest that there are two distinct sediment sources to Mattole Canyon (Figure 5): a metasandstone clast-rich southern source with negative PC1 values delivered predominantly by the Mattole River; and a northern quartzose source with positive PC1 values fed from coastal creeks and bluffs. These findings are consistent with the mapping by Patsch and Griggs (2007). The two sources converge above the head of Mattole Canyon, where they mix and are staged for delivery into the canyon (Figure 7). Depending on wave direction and time of year, littoral sediment is transported to the north or south past the canyon head or converges near the canyon head (Figure 6B). This is consistent with provenance results showing northern and southern sources intermingling above the canyon head. Canyon bathymetry also induces significant sheltering of the shore adjacent to the Mattole headwall when waves impact the shore from west-northwest (270–310 degrees; Figure 6A), consistent with observed flat and fine-grained beach at the site. Interestingly, the width of the region of greatest sheltering is similar and collocated with the uppermost gullies of the Mattole Canyon headwall (Figure 6A), which could suggest a relationship between headwall form and sediment transport processes. We suggest that the high estimated sediment delivery to shore, sustained

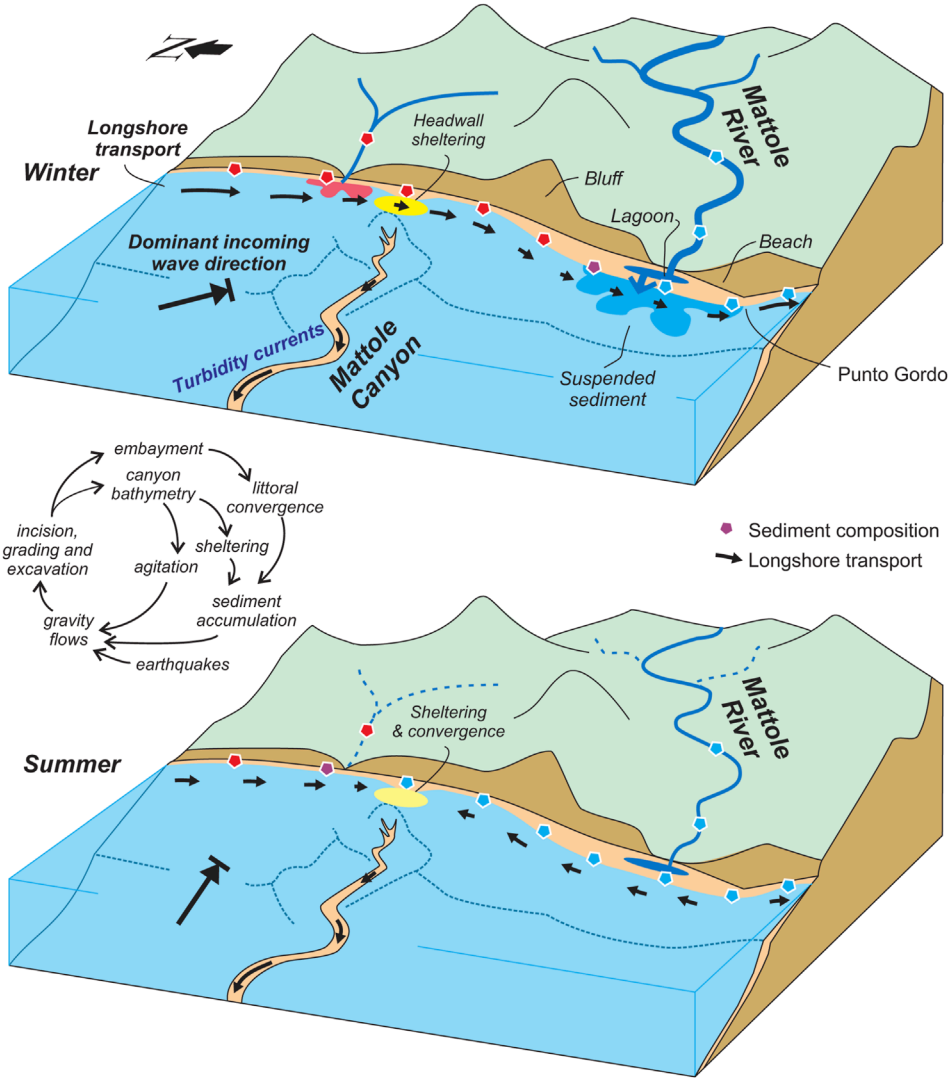

FIGURE 7
Conceptual diagram of Mattole Canyon system during winter and summer seasons, showing alternating longshore sediment disbursement due to changing wave direction and sediment supply to shore from rivers. Inset diagram illustrates hypothetical feedbacks between canyons, sediment transport, submarine gravity flows, and coast shape at a littorally-connected submarine canyon.

convergence, and sheltering should promote significant sediment accumulation in the headwall region. Further, large waves can on some occasions bring currents capable of mobilizing up to gravel-sized sediment into the canyon head, which are typically strongest during the winter months (Figure 6C).

The hypothesized convergence of longshore sediment at the Mattole Canyon head in tandem with the stable position of the adjacent shoreline over the last half century (cf. USGS Petrolia, CA quads of 1969 and 1997) implies a significant proportion of bed sediment entering the Mattole River littoral cell is diverted into Mattole Canyon. If, for example, half of the sediment delivered from the Mattole River and other streams entering the littoral cell passes through Mattole Canyon, this would imply 18,000 tons of bedload and 1 million tons of suspended load and passes into Mattole Canyon each year. Thin accumulation observed on the adjacent shelf (Beeson et al., 2017) implies a greater proportion of this sediment load transits the canyon, so these rough estimates of sediment delivered to Mattole Canyon are likely minimum estimates. These estimates assume zero leakage of sediment to or from the Eel River and Spanish Flats littoral cells.

4.1 Comparisons with other submarine canyons

At sixteen of the 20 shore-connected canyons across the Pacific coast of the contiguous U.S. river-delivered sediment must traverse the littoral cell to enter their headwalls (Smith et al., 2017). This sediment routing topology is shared by several other shore-intersecting canyons worldwide (Lewis and Barnes, 1999; Allin et al., 2016; Cerrillo-Escoriza et al., 2024), so the findings from Mattole Canyon described here may be applicable more broadly to a general understanding of the maintenance and onshore connection of active submarine canyons supplied by littoral transport. At

Kaikōura Canyon offshore New Zealand, littoral sediment enters the canyon's headwalls from the south, which has led to many recent sandy turbidites that transit only the uppermost canyon (1,400 m), but these events are dwarfed by rare seismically-generated sediment gravity events, which traveled >1,500 km out to the Hikurangi Channel to the deep sea, created significant scours into bedrock, and moved significant volumes of coarse sediment (Lewis and Barnes, 1999; Mountjoy et al., 2018). A similar pattern emerges at shore-connected Nazaré Canyon offshore Portugal, where smaller turbidity currents triggered by waves are common in the upper canyon, but are remobilized and scoured by rare high-magnitude "flushing" episodes that transport significant volumes of sediment to the deep sea (Allin et al., 2016).

Submarine canyons offshore Northern California and Oregon have predominantly become disconnected from littoral bedload fluxes due to the post-glacial transgression, with most canyon heads occurring near the 100 m isobath (Goldfinger et al., 2007). Observations from canyons near to Mattole Canyon nevertheless provide insight into what likely occurs there. Eel Canyon incises the shelf 50 km north of Mattole Canyon and is the best studied submarine canyon in the region. Its headwall extends to 100 m depth, and was shown to have accumulated up to 6 cm/yr of fine sediment over a decade, with the thickest accumulations focused in canyon head gullies (Mullenbach and Nittrour, 2006). This sediment is likely delivered to the canyon head by resuspension and fluidization of muddy sediment during storms (Puig et al., 2003). Only 12% of Eel River sediment enters Eel Canyon (Mullenbach et al., 2004), and virtually no bedload sediment. Holocene turbidites sampled in the Eel Channel are, fine-grained, and correlate to well-documented high-magnitude seismic events (Goldfinger et al., 2012). The Trinidad, Klamath, and Smith canyons to the north of Eel Canyon similarly have headwalls near the last-glacial shoreline (Figure 1B), and have only produced turbidity currents during major earthquakes along the Cascadia megathrust (Goldfinger et al., 2012). Mendocino Canyon occurs less than 10 km north of that of Mattole Canyon, at the 100 m isobath (Figure 2A). Despite its apparent disconnection from littoral sediment supply, dilute turbidity currents have been observed by ROV in its thalweg at 400 m depth (Sumner and Paull, 2014), suggesting it received fine-grained sediment much like Eel Canyon.

South of Punto Gordo, multiple canyons join down-gradient with the deep Viscaino Channel (Figure 1B). Of these canyons, only Delgada Canyon extends to the littoral cell (Figure 2A), and the other canyons only discharge turbidity currents due to major earthquakes along the San Andreas Fault zone (Goldfinger et al., 2007). Since their headwalls are of roughly the same size and receives a similar sediment supply from shore, sediment volumes discharged from Delgada Canyon provides a useful analog for the volumes required to fill and discharge the sediment "capacitor" in the head of Mattole Canyon (Covault and Fildani, 2014). Delgada Canyon incises the shelf, is connected to the Shipman Flats littoral cell south of Mattole Canyon, and collects sediment supplied from several steep coastal streams (Figure 1A). Repeat multibeam surveys of the headwall of Delgada Canyon show significant bathymetric change between 2008 and 2015 (Smith et al., 2018), with up to 10 m of erosion in the headwall and coeval migration of sand waves in the canyon's uppermost thalweg (Smith et al., 2018). A conservative estimate of 18,000 tons of bedload/year that is diverted into Mattole Canyon would be enough to refill the volume loss observed in Delgada Canyon every 2 years, on average. This suggests that geomorphically significant events are also likely to occur in Mattole Canyon several times per decade, if not more frequently, i.e., annually or sub-annually, due to higher sediment supply from the Mattole River. This is consistent with the sediment waves observed in the thalweg in the upper 300 m depth of its thalweg that imply the recent passage of turbidity currents (Figure 2C), though similar bedforms may be created by internal tides and other processes (Cacchione et al., 2002; Puig et al., 2013; Puig et al., 2014). Possible triggering mechanisms for turbidity currents include seismicity, which is common at the Mendocino Triple Junction (Figure 1A), direct agitation by waves (Smith et al., 2018), the settling of sediment plumes generated by wave agitation and river floods (Puig et al., 2003; Talling et al., 2015), and autogenic retro-gradational mass failure of fine sand (Mastbergen and Van den Berg, 2003). While no observation record exists for which of these processes operate and when, significant to all is the sediment supplied to the site from the Mattole River. The discharge of which scales to the magnitude of winter flood events and can vary significantly within a typical year and at decadal timescales (Figure 6C).

A thick (76 m) package of ROV-observed, ^{14}C-dated strata composed of Early Holocene sandy turbidites that is exposed in large scours in the lower Eel Channel and documented by Paull et al. (2014) provides an additional analogy for the processes expected at a shore-connected system like Mattole Canyon. These strata were deposited at a rate of 1.6 cm/yr during the end of the last glaciation (Paull et al., 2014), when glacial climate-enhanced sediment transport from the Eel River (Syvitski and Morehead, 1999) was delivered regularly to the Eel Canyon headwall. The rate of sediment accumulation in the Mendocino Channel (0.6 cm/yr) is the highest observed in the submarine channels offshore Northern California and Oregon (Figure 1B), and most closely resembles the Early Holocene Eel system.

Based on observed provenance results, wave modeling, the Mattole River flood record, and repeat Sentinel-2 imagery, we envision a dynamic linked Mattole River – Mattole Canyon system that is variably connected by littoral sediment transport at different times of year depending on wave conditions and floods (Figure 7). In winter, the river is most active and delivers significant volumes of water and sediment at its outlet (Figure 6C). Typically, wave-driven littoral transport is south-directed or neutral during winter due to waves from the NW, away from Mattole Canyon, and accumulates near the outlet. This general pattern does not exclude rare but potentially geomorphically significant scenarios when suspended Mattole River flood sediment is directly entrained by waves and travels northward into the canyon head (Figure 3B). Plumes of river-delivered suspended sediment may also be the origin for the hanging tributary gullies that enter the Mattole Canyon thalweg from the direction of the Mattole River outlet (Figure 2C). In summer, Mattole River discharge declines and sediment delivery ceases at the outlet, but waves from the west work to move recently deposited sediment northward towards Mattole Canyon from the Mattole River outlet area.

Sediment accumulation is promoted at the Mattole Canyon head during all seasons by convergence due to the slight embayment at the site, and by sheltering resulting from wave refraction caused by interactions with canyon bathymetry. Sediment accumulation in the headwall region involves a steepening of the local slope, which likely leads to common mass failure events in the uppermost gullies of the canyon and associated turbidity currents that travel down-canyon. Sediment discharges from the canyon head can result

from myriad possible processes (e.g., waves, seismicity, littoral plume collapse, autogenic slope failure), all of which should be promoted by sediment accumulation. In this study, we model that wave agitation capable of mobilizing fine gravel and triggering sediment gravity flows occurs mostly during winter months (Figure 7). These waves would simultaneously agitate the adjacent shelf, where wave-supported fluid mud is likely generated (Puig et al., 2003). These findings suggest possible feedback between canyon occurrence and embayment, wave-generated littoral convergence, and the net export of sediment from the littoral cell. Sediment export into the canyon may also contribute to enhanced coastal erosion adjacent to the canyon head (Carter et al., 1987; Tiede et al., 2023) and thus promote littoral convergence at the site due to increased embayment of the shore (Figure 7).

We hypothesize that the resulting turbidity currents in the uppermost canyon head act to incise and grade the canyon's meandering upper thalweg and shape the observed sediments waves. Some of these events may travel down-canyon a significant distance, however, and some are likely deposited in the uppermost kilometer of the canyon. Large magnitude earthquakes have generated some of the greatest magnitude and longest-travelled recorded turbidity current events (Goldfinger et al., 2007; Mountjoy et al., 2018). Seismicity is common at the Mendocino Triple Junction and is very likely a trigger for turbidity currents in Mattole Canyon (Figure 1A). However, while the site is very seismically active, the accumulation of 36 sandy turbidites across 830 years in the Mendocino Channel at 2,621 m depth (Goldfinger et al., 2012) also raises the possibility that some of these long-traveled events may have a non-seismic trigger. If this were the case, environmental signals from the shore are not fully stripped from the Mattole Canyon-Mendocino Channel system record (Romans et al., 2016). It remains possible, for example, that the ENSO-driven oscillations in sediment transport observed in many California rivers (Andrews and Antweiler, 2012) are also recorded in the deep sea.

5 Conclusions

We investigated the Mattole River littoral cell and Mattole submarine canyon of Northern California to better evaluate the likelihood of the transport of littoral grade sediment into the headwall region of a shore-connected submarine canyon system. In this remote and data-poor region of the California shoreline, we used a combination of methods including field sampling, sediment geochemistry, and numerical wave modeling. Sediment waves in the uppermost 300 m of the canyon imply active sediment transport events, and the rapid Late Holocene accumulation of multiple sandy turbidites at 2,621 m water depth in Mendocino Channel suggests that littoral material regularly transits from the shore to the deep sea. Wave modeling also indicates that refraction over steep canyon bathymetry acts to shelter the adjacent shore from the largest winter waves, possibly promoting sediment accumulation at the site, and can periodically induce sediment mobilizing currents in the uppermost canyon. Provenance evidence and wave modeling of the shore adjacent to the Mattole submarine canyon indicate that it is fed by converging littoral sediment streams from north and south. Quartz-rich sediment from the north with high PC1 values is clearly distinguished from lithic sediment with low PC1 values delivered by the Mattole River. These sediment sources were observed to converge adjacent to the Mattole Canyon headwall, suggesting that a significant proportion of the sediment delivered to the shore by the Mattole River is routed into Mattole Canyon. Lastly, we outline a conceptual model for the wider implications of direct littoral sediment supply and wave-driven agitation to submarine canyon headwalls (Figure 7). The prevalence of active submarine canyons in a tectonically active region with high sediment supply supports the hypothesis that canyon incision is favored in such places over longer timescales. Cross-shore sediment fluxes are further encouraged by canyon bathymetry and coastal embayment. Associated gravity flow events help to maintain a connection to the littoral sediment stream through the incision and grading of submarine channels. Coastal erosion and embayment of the shoreline are further promoted adjacent to canyon heads due to net sediment export off the shelf.

Data availability statement

The original contributions presented in the study are included in the article/Supplementary Material; further inquiries can be directed to the corresponding author.

Author contributions

SJ: Writing–original draft, Writing–review and editing. MS: Writing–original draft, Writing–review and editing. DB: Writing–original draft, Writing–review and editing. EM: Writing–original draft, Writing–review and editing.

Funding

The author(s) declare financial support was received for the research, authorship, and/or publication of this article. This study was made possible by research grants from Northern Arizona University and the Geological Society of America.

Acknowledgments

We thank F. Settanni for field and laboratory assistance. We appreciate the thoughful suggestions of Editor Ángel Puga-Bernabéu and three reviewers.

Conflict of interest

Author DB was employed by Marda Science LLC.

The remaining authors declare that the research was conducted in the absence of any commercial or financial relationships that could be construed as a potential conflict of interest.

Publisher's note

All claims expressed in this article are solely those of the authors and do not necessarily represent those of

their affiliated organizations, or those of the publisher, the editors and the reviewers. Any product that may be evaluated in this article, or claim that may be made by its manufacturer, is not guaranteed or endorsed by the publisher.

Supplementary material

The Supplementary Material for this article can be found online at: https://www.frontiersin.org/articles/10.3389/feart.2024.1377997/full#supplementary-material

References

Allin, J. R., Hunt, J. E., Talling, P. J., Clare, M. A., Pope, E., and Masson, D. G. (2016). Different frequencies and triggers of canyon filling and flushing events in Nazaré Canyon, offshore Portugal. *Mar. Geol.* 371, 89–105. doi:10.1016/j.margeo.2015.11.005

Amarouche, K., Akpınar, A., Soran, M. B., Myslenkov, S., Majidi, A. G., Kankal, M., et al. (2021). Spatial calibration of an unstructured SWAN model forced with CFSR and ERA5 winds for the Black and Azov Seas. *Appl. Ocean Res.* 117, 102962. doi:10.1016/j.apor.2021.102962

Andrews, E. D., and Antweiler, R. C. (2012). Sediment fluxes from California coastal rivers: the influences of climate, geology, and topography. *J. Geol.* 120, 349–366. doi:10.1086/665733

Arzola, R. G., Wynn, R. B., Lastras, G., Masson, D. G., and Weaver, P. P. E. (2008). Sedimentary features and processes in the Nazaré and Setúbal submarine canyons, west Iberian margin. *Mar. Geol.* 250, 64–88. doi:10.1016/j.margeo.2007.12.006

Bascom, W. N. (1951). The relationship between sand size and beach-face slope. *Eos Trans. AGU* 32, 866–874. doi:10.1029/TR032i006p00866

BDSN (2014). Berkeley digital seismic network. *UC Berkeley Seismol. Lab. Dataset*. doi:10.7932/BDSN

Beeson, J. W., Johnson, S. Y., and Goldfinger, C., 2017, The transtensional offshore portion of the northern San Andreas fault: fault zone geometry, late Pleistocene to Holocene sediment deposition, shallow deformation patterns, and asymmetric basin growth: *Geosphere*, v. 13, 173–181. doi:10.1130/GES01388.1

Bernhardt, A., and Schwanghart, W. (2021). Where and why do submarine canyons remain connected to the shore during sea-level rise? Insights from global topographic analysis and Bayesian regression. *Geophys. Res. Lett.* 48, e2020GL092234. doi:10.1029/2020gl092234

Beyramzadeh, M., Siadatmousavi, S. M., and Derkani, M. H. (2021). Calibration and skill assessment of two input and dissipation parameterizations in WAVEWATCH-III model forced with ERA5 winds with application to Persian Gulf and Gulf of Oman. *Ocean. Eng.* 219, 108445. doi:10.1016/j.oceaneng.2020.108445

Booij, N., Ris, R. C., and Holthuijsen, L. H. (1999). A third-generation wave model for coastal regions: 1. Model description and validation. *J. Geophys. Res. Oceans* 104, 7649–7666. doi:10.1029/98JC02622

Buscombe, D. (2020). SediNet: a configurable deep learning model for mixed qualitative and quantitative optical granulometry. *Earth Surf. Process. Landforms* 45, 638–651. doi:10.1002/esp.4760

Buscombe, D., and Conley, D. C. (2012). Effective shear stress of graded sediments. *Water Resour. Res.* 48, W05506. doi:10.1029/2010WR010341

Cacchione, D. A., Pratson, L. F., and Ogston, A. S. (2002). The shaping of continental slopes by internal tides. *Science* 296, 724–727. doi:10.1126/science.1069803

Carter, R. W. G., Johnston, T. W., McKenna, J., and Orford, J. D. (1987). Sea-level, sediment supply and coastal changes: examples from the coast of Ireland. *Prog. Oceanogr.* 18, 79–101. doi:10.1016/0079-6611(87)90027-9

Cerrillo-Escoriza, J., Lobo, F. J., Puga-Bernabéu, Á., Bárcenas, P., Mendes, I., Pérez-Asensio, J. N., et al. (2024). Variable downcanyon morphology controlling the recent activity of shelf-incised submarine canyons (Alboran Sea, western Mediterranean). *Geomorphology* 453, 109127. doi:10.1016/j.geomorph.2024.109127

Chapman, K. A., Best, R. J., Smith, M. E., Mueller, E. R., Grams, P. E., and Parnell, R. A. (2021). Estimating the contribution of tributary sand inputs to controlled flood deposits for sandbar restoration using elemental tracers, Colorado River, Grand Canyon National Park, Arizona. *Geol. Soc. Am. Bull.* 133, 1141–1156.

Chen, Y., Parsons, D. R., Simmons, S. M., Williams, R., Cartigny, M. J., Hughes Clarke, J. E., et al. (2021). Knickpoints and crescentic bedform interactions in submarine channels. *Sedimentology* 68 (1), 1358–1,377. doi:10.1111/sed.12886

Clare, M. A., Hughes Clarke, J. E., Talling, P. J., Cartigny, M. J. B., and Pratomo, D. G. (2016). Preconditioning and triggering of offshore slope failures and turbidity currents revealed by most detailed monitoring yet at a fjord-head delta. *Earth Planet. Sci. Lett.* 450, 208–220. doi:10.1016/j.epsl.2016.06.021

Covault, J. A., and Fildani, A. (2014). Chapter 23 Continental shelves as sediment capacitors or conveyors: source-to-sink insights from the tectonically active Oceanside shelf, southern California, USA. *Geol. Soc. Lond. Memoirs* 41 (1), 315–326. doi:10.1144/m41.23

Covault, J. A., Kostic, S., Paull, C. K., Ryan, H. F., and Fildani, A. (2014). Submarine channel initiation, filling and maintenance from sea-floor geomorphology and morphodynamic modelling of cyclic steps. *Sedimentology* 61 (1), 1031–1054. 031–1,054. doi:10.1111/sed.12084

Covault, J. A., Kostic, S., Paull, C. K., Sylvester, Z., and Fildani, A. (2017). Cyclic steps and related supercritical bedforms: building blocks of deep-water depositional systems, western North America. *Mar. Geol.* 393, 4–20. doi:10.1016/j.margeo.2016.12.009

Covault, J. A., Romans, B. W., Graham, S. A., Fildani, A., and Hilley, G. E. (2011) "Terrestrial source to deep-sea sink sediment budgets at high and low sea levels: insights from tectonically active Southern California,"*Geology*, 39, 619–622. doi:10.1130/g31801.1

Dibblee, T. W. (2008). Geologic map of the Cape Mendocino & scotia 15 minute quadrangles. *Humboldt. Cty. Calif. Dibblee Found. Map*.

Dickinson, W. R., and Snyder, W. S. (1979). Geometry of triple junctions related to San Andreas transform. *J. Geophys. Res.* 84 (B2), 561–572. doi:10.1029/jb084ib02p00561

Dumitru, T. A. (1991). Major quaternary uplift along the northernmost san Andreas Fault, king range, northwestern California: geology. *Geol.* 19, 526–529. doi:10.1130/0091-7613(1991)019<0526:mquatn>2.3.co;2

Furlong, K. P., and Schwartz, S. Y. (2004). Influence of the Mendocino triple junction on the tectonics of coastal California: annual review of earth. *Planet. Sci.* 32, 403–433. doi:10.1146/annurev.earth.32.101802.120252

Gardner, V. J. (2017). The morphometry of the deep-water sinuous Mendocino Channel and the immediate environs, northeastern Pacific Ocean. *Geosciences* 7, 124. doi:10.3390/geosciences7040124

Goldfinger, C., Morey, A. E., Nelson, C. H., Gutiérrez-Pastor, J., Johnson, J. E., Karabanov, E., et al. (2007). Rupture lengths and temporal history of significant earthquakes on the offshore and north coast segments of the Northern San Andreas Fault based on turbidite stratigraphy. *Earth Planet. Sci. Lett.* 254, 9–27. doi:10.1016/j.epsl.2006.11.017

Goldfinger, C., Nelson, C. H., Morey, A. E., Johnson, J. E., Patton, J. R., Karabanov, E. B., et al. (2012). Turbidite event history—methods and implications for Holocene paleoseismicity of the Cascadia subduction zone. *USGS Prof. Pap.* doi:10.3133/PP1661F

Gorrell, L., Raubenheimer, B., Elgar, S., and Guza, R. T. (2011). SWAN predictions of waves observed in shallow water onshore of complex bathymetry. *Coast. Eng.* 58, 510–516. doi:10.1016/j.coastaleng.2011.01.013

Guiastrennec-Faugas, L., Gillet, H., Peakall, J., Dennielou, B., Gaillot, A., and Jacinto, R. S. (2021). Initiation and evolution of knickpoints and their role in cut-and-fill processes in active submarine channels. *Geology* 49, 314–319. doi:10.1130/g48369.1

Hage, S., Cartigny, M. J., Sumner, E. J., Clare, M. A., Hughes Clarke, J. E., Talling, P. J., et al. (2019), Direct monitoring reveals initiation of turbidity currents from extremely dilute river plumes: *Geophys. Res. Lett.*, v. 46. 11,11310–11320. doi:10.1029/2019gl084526

Hallermeier, R. J. (1981). A profile zonation for seasonal sand beaches from wave climate. *Coast. Eng.* 4, 253–277. doi:10.1016/0378-3839(80)90022-8

Hansen, J. E., Raubenheimer, B., Elgar, S., List, J. H., and Lippmann, T. C., 2017, Physical linkages between an offshore canyon and surf zone morphologic change: *J. Geophys. Res. Oceans*. 122, 3451–3460. doi:10.1002/2016jc012319

Hansen, J. E., Raubenheimer, B., List, J. H., and Elgar, S., 2015, Modeled alongshore circulation and force balances onshore of a submarine canyon: *J. Geophys. Res. Oceans*, v. 120, 1887–1903. doi:10.1002/2014JC010555

Hersbach, H., Bell, B., Berrisford, P., Hirahara, S., Horányi, A., Muñoz-Sabater, J., et al. (2020). The ERA5 global reanalysis. *Q. J. R. Meteorological Soc.* 146 (1), 1999–2,049. doi:10.1002/qj.3803

Johnson, S. Y., Cochrane, G. R., Golden, N. E., Dartnell, P., Hartwell, S. R., Cochran, S. A., et al. (2017). The California seafloor and coastal mapping program–Providing science and geospatial data for California's state waters. *Ocean Coast. Manag.* 140, 88–104. doi:10.1016/j.ocecoaman.2017.02.004

Kemper, J. T., Rathburn, S. L., Friedman, J. M., Nelson, J. M., Mueller, E. R., and Vincent, K. R. (2022). Fingerprinting historical tributary contributions to floodplain sediment using bulk geochemistry. *Catena* 214, 106231. doi:10.1016/j.catena.2022.106231

Lamb, M. P., Parsons, J. D., Mullenbach, B. L., Finlayson, D. P., Orange, D. L., and Nittrouer, C. A. (2008) "Evidence for superelevation, channel incision, and formation of cyclic steps by turbidity currents in Eel Canyon, California,"*Geol. Soc. Am. Bull.*, 120, 463–475. doi:10.1130/b26184.1

Lewis, K. B., and Barnes, P. M. (1999). Kaikoura Canyon, New Zealand: active conduit from near-shore sediment zones to trench-axis channel. *Mar. Geol.* 162, 39–69. doi:10.1016/s0025-3227(99)00075-4

Lintern, D. G., Hill, P. R., and Stacey, C. (2016). Powerful unconfined turbidity current captured by cabled observatory on the Fraser River delta slope, British Columbia, Canada. *Sedimentology* 63, 1041–1064. doi:10.1111/sed.12262

Lock, J., Kelsey, H., Furlong, K., and Woolace, A. (2006). Late Neogene and quaternary landscape evolution of the northern California coast ranges: evidence for Mendocino triple junction tectonics. *Geol. Soc. Am. Bull.* 118 (1), 1232–1,246. doi:10.1130/b25885.1

Long, J. W., and Özkan-Haller, H. T. (2005). Offshore controls on nearshore rip currents. *J. Geophys. Res.* 110, C12007. doi:10.1029/2005JC003018

Long, J. W., and Özkan-Haller, H. T. (2016). Forcing and variability of nonstationary rip currents. *J. Geophys. Res. Oceans* 121, 520–539. doi:10.1002/2015jc010990

Magne, R., Belibassakis, K. A., Herbers, T. H. C., Ardhuin, F., O'Reilly, W. C., and Rey, V. (2007). Evolution of surface gravity waves over a submarine canyon. *J. Geophys. Res.* 112 . doi:10.1029/2005JC003035

Mastbergen, D. R., and Van Den Berg, J. H. (2003). Breaching in fine sands and the generation of sustained turbidity currents in submarine canyons. *Sedimentology* 50, 625–637.

McLaughlin, R. J., Ellen, S. D., Blake, M. C., Jayco, A. S., Irwin, W. P., and Alto, R. (2000). *Geology of the Cape Mendocino, Eureka, Garberville, and southwestern part of the Hayfork 30 x 60 minute quadrangles and adjacent offshore area*. USA: U.S. Geological Survey. Map MF-2000.

McLaughlin, R. J., Kling, S. A., Poore, R. Z., McDougall, K., and Beutner, E. C. (1982). Post-middle Miocene accretion of Franciscan rocks, northwestern California. *GSA Bull.* 93, 595–605. doi:10.1130/0016-7606(1982)93<595:pmaofr>2.0.co;2

McLaughlin, R. J., Lajoie, K. R., Sorg, D. H., Morrison, S. D., and Wolfe, J. A. (1983). Tectonic uplift of a middle Wisconsin marine platform near the Mendocino triple junction, California. *Calif. Geol.* 11, 35–39. doi:10.1130/0091-7613(1983)11<35:tuoamw>2.0.co;2

Merritts, D., and Bull, W. B. (1989). Interpreting Quaternary uplift rates at the Mendocino triple junction, northern California, from uplifted marine terraces. *Geology* 17, 1020–1024. doi:10.1130/0091-7613(1989)017<1020:iqurat>2.3.co;2

Moon, S., Perron, J. T., Martel, S. J., Holbrook, W. S., and St. Clair, J. (2018). A model of three-dimensional topographic stresses with implications for bedrock fractures, surface processes, and landscape evolution. *J. Geophys. Res. Earth Surf.* 502, 156–165. doi:10.1016/j.epsl.2018.09.006

Mountjoy, J. J., Howarth, J. D., Orpin, A. R., Barnes, P. M., Bowden, D. A., Rowden, A. A., et al. (2018). Earthquakes drive large-scale submarine canyon development and sediment supply to deep-ocean basins. *Sci. Adv.* 4. doi:10.1126/sciadv.aar3748

Mueller, E. R., Smith, M. E., and Pitlick, J. (2016). Lithology-controlled evolution of stream bed sediment and basin-scale sediment yields in adjacent mountain watersheds, Idaho, USA. *Earth Surf. Process. Landforms* 41 (1), 1869–1,883. doi:10.1002/esp.3955

Mullenbach, B. L., and Nittrouer, C. A. (2006). Decadal record of sediment export to the deep sea via Eel Canyon. *Cont. Shelf Res.* 26 (2), 2157–2177. 157–2,177. doi:10.1016/j.csr.2006.07.019

Mullenbach, B. L., Nittrouer, C. A., Puig, P., and Orange, D. L. (2004). Sediment deposition in a modern submarine canyon: Eel Canyon, northern California. *Mar. Geol.* 211, 101–119. doi:10.1016/j.margeo.2004.07.003

Normandeau, A., Bourgault, D., Neumeier, U., Lajeunesse, P., St-Onge, G., Gostiaux, L., et al. (2019). Storm-induced turbidity currents on a sediment-starved shelf: Insight from direct monitoring and repeat seabed mapping of upslope migrating bedforms. *Sedimentology* 67, 1045–1068.

Ortega-Sánchez, M., Lobo, F. J., López-Ruiz, A., Losada, M. A., and Fernández-Salas, L. M. (2014). The influence of shelf-indenting canyons and infralittoral prograding wedges on coastal morphology: the Carchuna system in Southern Spain. *Mar. Geol.* 347, 107–122. doi:10.1016/j.margeo.2013.11.006

Palanques, A., Guillén, J., Puig, P., and Durrieu de Madron, X. (2008). Storm-driven shelf-to-canyon suspended sediment transport at the southwestern Gulf of Lions. *Cont. Shelf Res.* 28, 1947–1956.

Patsch, K., and Griggs, G. B. (2007). *Development of sand budgets for California's major littoral cells: California Coastal Records Project*, 1–115.

Paull, C. K., Caress, D. W., Ussler III, W., Lundsten, E., and Meiner-Johnson, M., 2011, High-resolution bathymetry of the axial channels within Monterey and Soquel submarine canyons, offshore central California: *Geosphere*, v. 7, 101.

Paull, C. K., McGann, M., Sumner, E. J., Barnes, P. M., Lundsten, E. M., Anderson, K., et al. (2014). Sub-decadal turbidite frequency during the early Holocene: Eel Fan, offshore northern California. *Geology* 42, 855–858. doi:10.1130/g35768.1

Paull, C. K., Ussler, W. I. I., Greene, H. G., Keaten, R., Mitts, P., and Barry, J. (2003). Caught in the act: the 20 December 2001 gravity flow event in Monterey Canyon. *Geo-Marine Lett.* 22, 227–232. doi:10.1007/s00367-003-0117-2

Pratson, L. F., and Coakley, B. J. (1996). A model for the headward erosion of submarine canyons induced by downslope-eroding sediment flows. *Geol. Soc. Am. Bull.* 108, 225–234. doi:10.1130/0016-7606(1996)108<0225:amfthe>2.3.co;2

Puig, P., Greenan, B. J. W., Li, M. Z., Prescott, R. H., and Piper, D. J. W. (2013). Sediment transport processes at the head of Halibut Canyon, eastern Canada margin: an interplay between internal tides and dense shelf-water cascading. *Mar. Geol.* 341, 14–28. doi:10.1016/j.margeo.2013.05.004

Puig, P., Ogston, A. S., Mullenbach, B. L., Nittrouer, C. A., and Sternberg, R. W. (2003). Shelf-to-canyon sediment-transport processes on the Eel continental margin (northern California). *Mar. Geol.* 193, 129–149. doi:10.1016/s0025-3227(02)00641-2

Puig, P., Palanques, A., and Martín, J. (2014). Contemporary sediment-transport processes in submarine canyons. *Annu. Rev. Mar. Sci.* 6, 53–77. doi:10.1146/annurev-marine-010213-135037

Romans, B. W., Castelltort, S., Covault, J. A., Fildani, A., and Walsh, J. P. (2016). Environmental signal propagation in sedimentary systems across timescales. *Earth-Science Rev.* 153, 7–29. doi:10.1016/j.earscirev.2015.07.012

Romans, B. W., Fildani, A., Hubbard, S. M., Covault, J. A., Fosdick, J. C., and Graham, S. A. (2011). Evolution of deep-water stratigraphic architecture, Magallanes Basin, Chile. *Mar. Petroleum Geol.* 28, 612–628. doi:10.1016/j.marpetgeo.2010.05.002

Sayre, R., Noble, S., Hamann, S., Smith, R., Wright, D., Breyer, S., et al. (2019). A new 30 meter resolution global shoreline vector and associated global islands database for the development of standardized ecological coastal units. *J. Operational Oceanogr.* 12 (Suppl. 2), S47–S56. doi:10.1080/1755876x.2018.1529714

Sequeiros, O. E., Spinewine, B., Beaubouef, R. T., Sun, T., Garcia, M. H., and Parker, G., 2010, Bedload transport and bed resistance associated with density and turbidity currents: *Sedimentology*, v. 57, 1463–1490. doi:10.1111/j.1365-3091.2010.01152.x

Shepard, F. P. (1981). Submarine canyons: multiple causes and long-time persistence. *AAPG Bull.* 65, 1062–1077. doi:10.1306/03b59459-16d1-11d7-8645000102c1865d

Smith, M. E., Finnegan, N. J., Mueller, E. R., and Best, R. J., 2017, Durable terrestrial bedrock predicts submarine canyon formation: *Geophys. Res. Lett.*, v. 44,332–410. doi:10.1002/2017gl075139

Smith, M. E., Werner, S. H., Buscombe, D., Finnegan, N. J., Sumner, E. J., and Mueller, E. R., 2018, Seeking the shore: evidence for active submarine canyon head incision due to coarse sediment supply and focusing of wave energy: *Geophys. Res. Lett.*, v. 45, 403–412. doi:10.1029/2018GL080396

Sumner, E. J., and Paull, C. K. (2014). RSwept away by a turbidity current in Mendocino submarine canyon, California. *Geophys. Res. Lett.* 41, 7611–7618.

Swirad, Z. M., and Young, A. P. (2022). Spatial and temporal trends in California coastal cliff retreat. *Geomorphology* 412, 108318. doi:10.1016/j.geomorph.2022.108318

Symons, W. O., Sumner, E. J., Talling, P. J., Cartigny, M. J. B., and Clare, M. A. (2016). Large-scale sediment waves and scours on the modern seafloor and their implications for the prevalence of supercritical flows. *Mar. Geol.* 371, 130–148. doi:10.1016/j.margeo.2015.11.009

Syvitski, J. P., and Morehead, M. D. (1999). Estimating river-sediment discharge to the ocean: application to the Eel margin, northern California. *Mar. Geol.* 154, 13–28. doi:10.1016/s0025-3227(98)00100-5

Talling, P. J. (2014). On the triggers, resulting flow types and frequencies of subaqueous sediment density flows in different settings. *Mar. Geol.* 352, 155–182. doi:10.1016/j.margeo.2014.02.006

Talling, P. J., Allin, J., Armitage, D. A., Arnott, R. W. C., Cartigny, M. J. B., Clare, M. A., et al. (2015). Key future directions for research on turbidity currents and their deposits. *J. Sediment. Res.* 85, 153–169. doi:10.2110/jsr.2015.03

Thomson, J., Elgar, S., and Herbers, T. H. C. (2005). Reflection and tunneling of ocean waves observed at a submarine canyon. *Geophys. Res.* 32, 1–4.

Tiede, J., Jordan, C., Moghimi, A., and Schlurmann, T. (2023). Long-term shoreline changes at large spatial scales at the Baltic Sea: remote-sensing based assessment and potential drivers. *Front. mar. sci.* 10. doi:10.3389/fmars.2023.1207524

Tolman, H. L. (2009). *User manual and system documentation of WAVEWATCH III version 3.14, tech. Rep. 276, NOAA/NWS/NCEP/marine modeling and analysis branch*, Md. Germany: Camp Springs.

Van Rijn, L. C. (2014). A simple general expression for longshore transport of sand, gravel and shingle. *Coast. Eng.* 90, 23–39. doi:10.1016/j.coastaleng.2014.04.008

Vitousek, S. (2023). CoSMoS-COAST: the coastal, one-line, assimilated, simulation tool of the coastal storm modeling system. *U.S. Geol. Surv. Softw. release*. doi:10.5066/P95T9188

Vitousek, S., Vos, K., Splinter, K. D., Erikson, L., and Barnard, P. L. (2023). A model integrating satellite-derived shoreline observations for predicting fine-scale shoreline response to waves and sea-level rise across large coastal regions. *J. Geophys. Res. Earth Surf.* 128, e2022JF006936. doi:10.1029/2022jf006936

Vos, K. (2023). Time-series of shoreline change along the pacific rim. *Zenodo* v1.4. doi:10.5281/zenodo.7758183

Vos, K., Harley, M. D., Turner, I. L., and Splinter, K. D. (2023). Pacific shoreline erosion and accretion patterns controlled by El Niño/Southern Oscillation. *Nat. Geosci.* 16, 140–146. doi:10.1038/s41561-022-01117-8

Warrick, J. A., George, D. A., Gelfenbaum, G., Ruggiero, P., Kaminsky, G. M., and Beirne, M. (2009). Beach morphology and change along the mixed grain-size delta of the dammed Elwha River, Washington. *Geomorphology* 111, 136–148. doi:10.1016/j.geomorph.2009.04.012

Warrick, J. A., Vos, K., Buscombe, D., Ritchie, A. C., and Curtis, J. A. (2023). A large sediment accretion wave along a Northern California littoral cell. *J. Geophys. Res. Earth Surf.* 128, e2023JF007135. doi:10.1029/2023jf007135

Wright, L. D., Short, A. D., and Green, M. O. (1985). Short-term changes in the morphodynamic states of beaches and surf zones: an empirical predictive model. *Mar. Geol.* 62, 339–364. doi:10.1016/0025-3227(85)90123-9

Wu, W., Liu, Z., Zhai, F., Li, P., Gu, Y., and Wu, K. (2021). A quantitative method to calibrate the SWAN wave model based on the whitecapping dissipation term. *Appl. Ocean Res.* 114, 102785. doi:10.1016/j.apor.2021.102785

Zijlema, M. (2010). Computation of wind-wave spectra in coastal waters with SWAN on unstructured grids. *Coast. Eng.* 57, 267–277. doi:10.1016/j.coastaleng.2009.10.011

Zijlema, M., and van der Westhuysen, A. J. (2005). On convergence behaviour and numerical accuracy in stationary SWAN simulations of nearshore wind wave spectra. *Coast. Eng.* 52, 237–256. doi:10.1016/j.coastaleng.2004.12.006